*Sensors and Materials*, Vol. 36, No. 11 (2024) 4607–4629
MYU Tokyo



S & M 3820

# Fault Diagnosis Algorithm of Bearings under Variable Operating Conditions Based on Multisource Sensor Fusion and Discriminant Space Optimization

Dongsheng Wu,[1*] Yihao Chen,[1] and Yifan Chen[1,2**]

[1]School of Automation and Electrical Engineering, Shenyang Ligong University, Shenyang 110159, China
[2]School of Computing, University of Portsmouth, PO13HE, UK

(Received April 3, 2024; accepted July 1, 2024)

***Keywords:*** fault diagnosis, bearings, meta-learning, autoencoder, data reconstruction

In bearing fault diagnosis, traditional deep learning methods often fall short of achieving satisfactory diagnostic accuracy under variable operating conditions. A critical phase in this process is data acquisition, which heavily relies on high-precision sensors to accurately capture the real-time operational state of the bearing ring. To address this, a diversified sensor fusion strategy has been proposed, encompassing various sensor types such as temperature, and acoustic sensors. The strategy allows for comprehensive monitoring of the bearing's state from multiple dimensions. Vibration sensors are responsible for detecting minute vibrations and abnormal vibration patterns during the bearing's operation. Temperature sensors monitor changes in the bearing ring's temperature to identify potential overheating issues, whereas acoustic sensors capture unusual noises that may indicate faults. From the collective data gathered by these sensors, a comprehensive view of the bearing's operational state can be obtained, significantly enhancing the accuracy of fault diagnosis. To tackle the issue of low diagnostic accuracy under variable working conditions, an algorithm combining the advantages of data reconstruction and discriminative space optimization, data deconstruction and meta-learning discriminative space optimization (DR-MLDSO), has been utilized. Additionally, by integrating a hybrid dual-channel attention mechanism into the feature extraction network, challenges arising from variable application scenarios and data quality issues have been effectively addressed. Faced with the challenge of insufficient sample size, a similarity-based meta-learning algorithm was employed to train the encoder. Furthermore, the introduction of new constraints in the loss function leads to an improved sparse denoising autoencoder that optimizes data reconstruction, effectively reducing noise while preserving key features. Finally, incorporating a self-attention mechanism enhances the model's diagnostic capabilities in noisy environments, achieving superior diagnostic performance under variable working conditions, even with small sample sizes.

*Corresponding author: e-mail: wuds@sylu.edu.cn
**Corresponding author: e-mail: yifan.chen@port.ac.uk
https://doi.org/10.18494/SAM5063

ISSN 0914-4935 
https://myukk.org/

## 1. Introduction

In intelligent manufacturing, the health status of bearings, which serve as the core components within rotating machinery, is integrally related to the unimpeded operation of the entire system. Under extreme operating conditions, bearings are prone to damage, and the collection of fault data not only poses a threat to the safety of operators but also leads to significant property losses.[1–3] Consequently, it is particularly important to develop efficient, accurate, and rapid methods for bearing fault diagnosis.

First, through preprocessing steps, denoising autoencoders (AEs) are used to remove noise and retain key features. Then, an enhanced feature extraction network captures key attributes from the preprocessed data, while data from various sensors are integrated for analysis and recognition. By reducing intraclass distance to aid in recognizing samples of the same category, the probability of misclassification is reduced. Increasing interclass distance to more clearly delineate the boundaries between different categories helps improve classification accuracy. Additionally, optimizing the feature space to make feature representations more generalizable reduces the risk of overfitting. Vibration sensors (Fig. 1) detect abnormal vibrations during bearing wear or failure, and by analyzing the frequency, amplitude, and waveform of vibration signals, the extent of damage can be inferred. Temperature sensors (Fig. 2) monitor changes in bearing temperature, with increases usually indicating poor lubrication, excessive load, or increased friction. Acoustic sensors (Fig. 3) capture abnormal sounds during bearing failure, and the spectral analysis of these acoustic signals can identify fault patterns such as spalling, pitting, and cracking.

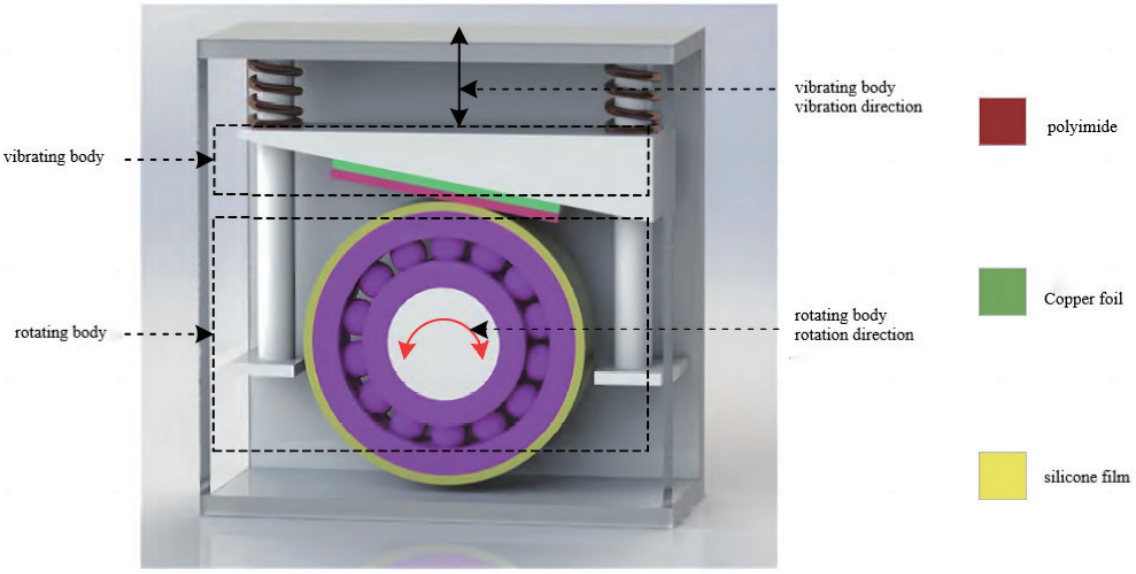


Fig. 1. (Color online) Vibration sensor.

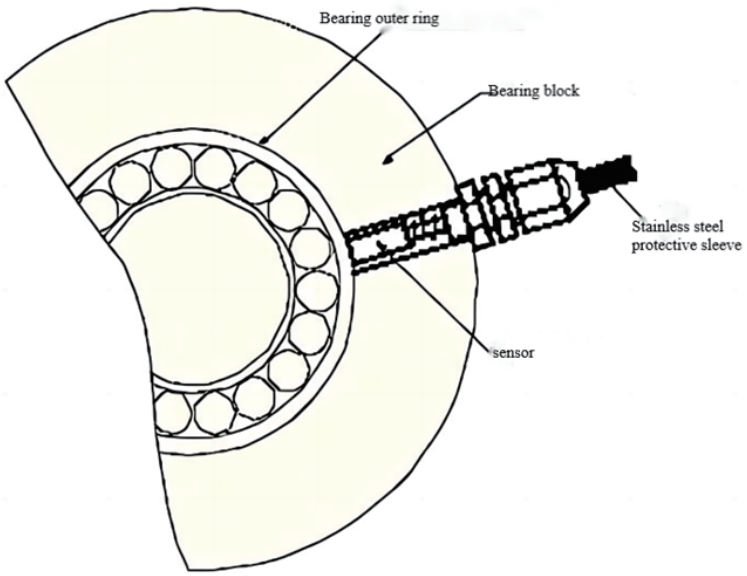


Fig. 2. (Color online) Temperature sensor.

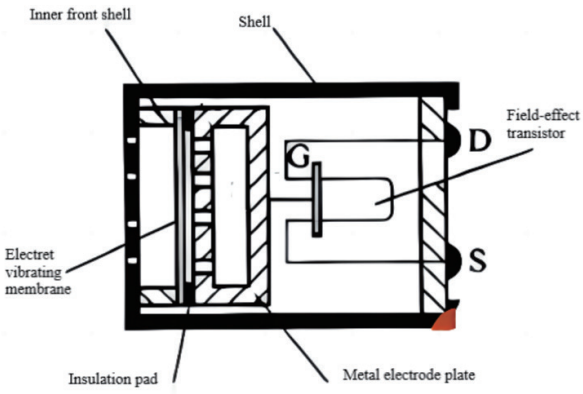


Fig. 3. (Color online) Acoustic sensor.

By combining data from vibration, temperature, and acoustic sensors, the fault diagnosis system can synchronously monitor the bearing status from multiple dimensions, allowing for comprehensive and in-depth fault analysis. This significantly improves the accuracy and speed of fault detection, ensuring the reliability of rotating machinery and the continuous operation of production lines.

Meta-learning models circumvent the need for the complex calculations and optimization of pretrained parameters, thus streamlining the training process. By exploiting the representational strength of pretrained models, meta-learning achieves swift generalization on new samples, thereby helping alleviate the problem of overfitting. These models can rapidly adapt to new tasks

using previously acquired knowledge, typically learning faster on new samples than traditional models trained from scratch. This is particularly beneficial in dealing with large datasets or situations that demand rapid adaptation to new circumstances. By harnessing the representational power of pretrained models, meta-learning can maintain good performance even with limited labeling data.

In the field of fault diagnosis, autoencoder (AE) models are primarily utilized for fault data representation and fault feature enhancement. Li *et al.*[4] developed a method for diagnosing faults in rotating machinery based on sparse AEs (SAEs), which was capable of extracting superior fault features through SAEs. Hasani *et al.*[5] investigated a method of standard AE-based correlation analysis with SAEs, achieving fault prediction in rotating machinery. However, in the presence of noise interference, the diagnostic accuracy of these methods can be compromised. Addressing this issue, Zhang *et al.*[6] leveraged deep convolutional networks to deeply mine features from vibration signals with noise interference, effectively diagnosing rolling bearing faults. Hoang and Kang[7] transformed vibration signals into grayscale images, and then used deep convolutional neural networks for feature extraction, achieving the effective recognition of rolling bearing faults under noise interference. However, because of the challenges of computational intensity, overfitting, and low diagnostic accuracy with small samples, they proposed the use of meta-learning models. Finn *et al.*'s[8] model-agnostic meta-learning (MAML) demonstrated significant generalization capabilities in image recognition. In time series classification tasks with extremely limited data, gradient-based meta-learning has been employed to classify unseen tasks. For problems of similarity recognition, metric learning has shown higher performance than meta-learning. Zhang *et al.*[9] applied Siamese neural networks based on metric learning to mechanical fault diagnosis, showing impressive performance. Matching networks, designed for single-image classification, employed long short-term memory networks to facilitate metric-based meta-learning, thus avoiding the need for fine-tuning when adapting to new tasks. Snell *et al.*[10] introduced prototypical networks (ProtoNets), a simple yet effective meta-learning-based approach suitable for small sample size image classification, with their experimental results validating the effectiveness of this method. Wang *et al.*[11] proposed a metric-based meta-learning model that combines conventional supervised learning with context-aware metric meta-learning, achieving good results in diagnosing faults in bearings and gearboxes. Experimental outcomes suggest that this method surpasses others, indicating it to be a promising approach under conditions of small sample size, high noise, and variable working conditions.

In this paper, we present a fault diagnosis method for bearings under variable operating conditions, utilizing data reconstruction and meta-learning discriminative space optimization (DR-MLDSO) in small sample situations. It denoises the raw data and extracts useful information hidden in it. This method is highly robust and enhances the feature extraction ability of the backbone network in meta-learning, enabling the model to converge rapidly under variable operating conditions and to have good diagnostic performance in small sample situations.

## 2. Related Principle

### 2.1 Improved sparse denoising autoencoder (SDAE)

In the realm of deep learning, data-driven methodologies, including AEs, have been developed for data reconstruction. AEs, as unsupervised learning models, minimize reconstruction error to approximate network outputs to inputs, essentially functioning as identity functions mapping outputs to inputs. A basic AE consists of a three-layer neural network with its middle layer capturing intelligent representations from raw data. Variants of AEs such as SAEs[12] and denoising AEs (DAEs)[13] have evolved under various constraints. SAEs, gaining prominence in fields such as machine learning and signal processing, implement sparsity by activating only a few nodes in each layer, enhancing effectiveness. DAEs blend noise into the original data, aiming to make the reconstructed output as close to the original as possible, thus bolstering the model's robustness against noise interference. The diagram of SAE and DAE is shown in Fig. 4.

Sparsity has become a popular concept in various fields such as machine learning, statistics, and signal processing. SAE is designed to impose regularization constraints on AE, primarily constraining the output of each layer to be sparse, where only a few nodes are activated. Sparse representation makes SAE more effective. DAE is also a variant of AE and introduces noise signals following specific distributions into the original data, generating new input data. The objective of DAE is to ensure that the reconstructed output data closely resembles the original input data, making the reconstructed results as consistent as possible with the original data and enhancing the model's robustness in noisy environments.

The following two encoders are introduced. The basic SAE consists of three layers: input, hidden, and output layers. They are built on top of the AE with sparse terms designed to suppress

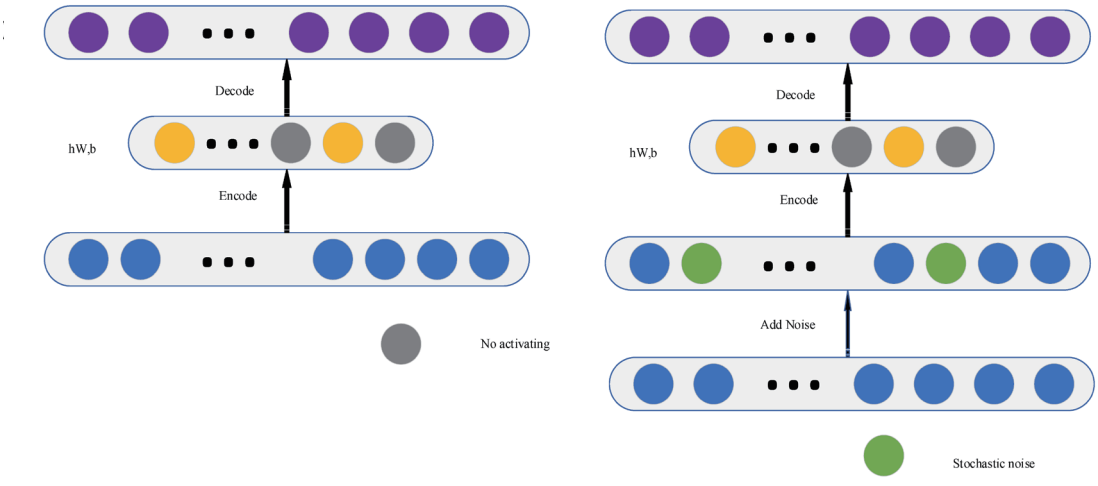


(a) (b)

Fig. 4. (Color online) (a) SAE. (b) DAE.

the output of the neural network nodes. Throughout the training, only a few nonzero elements participate in discerning obscured features from the original signal. In the following formulas, m represents the given sample, $x = [x_1, x_2, ..., x_n]$ represents the input, and $y = [y_1, y_2, ..., y_n]$ represents the output. The objective of the optimization is defined as

$$J_{SAE}(W,b) = \frac{1}{2m}\sum_{i=1}^{m}(\| h_{W,b}(x)^{(i)} - y^{(i)} \|^2) + \beta\sum_{j=1}^{s_1} KL(\rho \| \hat{\rho}_j), \tag{1}$$

where $\frac{1}{2m}\sum_{i=1}^{m}(\| h_{W,b}(x)^{(i)} - y^{(i)} \|^2)$ is the mean square error term. The sparse penalty term $\alpha$ is the penalty coefficient. $\beta$ is the sparsity parameter, which is generally set to 0.05, and $\hat{\rho}_j$ is the $j$th activation value of the hidden layer neuron. $\hat{\rho}_j = \rho$, $KL(\rho \| \hat{\rho}_j)$ denotes the relative entropy of the measurement of the distance between $\hat{\rho}_j$ and $\rho$.

$$KL(\rho \| \hat{\rho}_j) = \rho \log \frac{1-\rho}{1-\hat{\rho}_j} \tag{2}$$

DAE is an unsupervised learning method. In Fig. 5, the basic structure of DAE consists of an input layer, a hidden layer, and an output layer. The purpose of DAE is to try to approximate a constant function. DAE is more robust than AE. DAE has a mixture of random noise in the inputs, which mitigates the differences between the training and test datasets to some extent. Intuitively, DAE deals with two things: encoding the input for intrinsic information and removing the effects of the random noise applied to the AE input. The loss function of DAE is considered as a reconstructed log-likelihood function, defined as

$$-\log P(x \mid c(\tilde{x})), \tag{3}$$

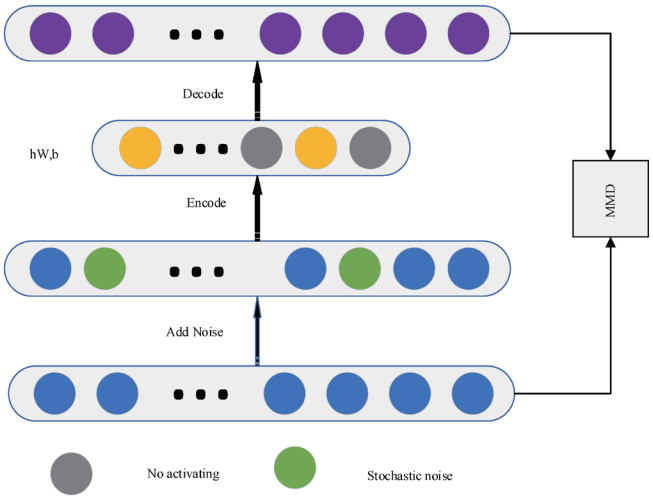


Fig. 5. (Color online) Improved SDAE structure diagram.

where $x$ is the raw data, $\tilde{x}$ is the randomly corrupted input, and $c(\tilde{x})$ is the code obtained using $\tilde{x}$. SDAE combines the sparse feature representation capabilities of SAE with the robustness of DAE. The loss criterion is to minimize the target loss function.

$$J_{SDAE}(W,b) = \frac{1}{2m}\sum_{i=1}^{m}(\| h_{W,b}(\tilde{x})^{(i)} - y^{(i)} \|^2) + \rho\sum_{j=1}^{s_1} KL(\rho \| \hat{\rho}_j) \tag{4}$$

SDAE integrates the advantages of both SAE and DAE. The mean squared error and sparsity penalty serve as the optimization objectives for the aforementioned data reconstruction methods. Note that the inputs $x = \{x^1, x^2, ..., x^i\}$ and outputs $y = \{y^1, y^2, ..., y^i\}$ are not considered to maintain consistency between the data obtained from $\hat{x}$ by SDAE and the original data.

The adoption of maximum mean discrepancy (MMD) can enhance the data reconstruction capability of SDAE. MMD is a statistical measure used to quantify the difference between the probability distributions of two samples. The modified structure of SDAE, incorporating MMD, is depicted in Fig. 5.

Assuming that samples a and b follow the probability distributions c and d, respectively, the MMD between these two samples can be defined as

$$MMD_k(X,Y) = \| E_p[\phi(x)] - E_Q[\phi(y)] \|^2_{H_k}. \tag{5}$$

Here, $H$ is the reproducing kernel Hilbert space (RKHS), $k$ is the characteristic nucleus, and $\phi(\bullet)$ is a nonlinear mapping from the original feature space to RKHS. It is not possible to obtain $E_p[\phi(x)]$ directly, but the mean can be used as a substitute since it is an unbiased estimate of the expectation. MMD can be expressed as

$$MMD_k(X,Y) = \| \frac{1}{n}\sum_{i=1}^{n}\phi(x_i) - \frac{1}{m}\sum_{j=1}^{1}\phi(y_i) \|^2. \tag{6}$$

However, as the spatial dimensions are exceedingly high, directly obtaining the unknown mapping $\phi(\bullet)$ is not feasible. Therefore, to resolve this issue, a characteristic nucleus with symmetric positive definite properties is introduced. Empirical MMD estimates can be calculated as

$$MMD_k(X,Y) = \frac{1}{n^2}\sum_{i=1}^{n}\sum_{j=1}^{n}k(x_i,x_j) - \frac{2}{mn}\sum_{i=1}^{n}\sum_{j=1}^{m}k(x_i,y_j) + \frac{1}{m^2}\sum_{i=1}^{n}\sum_{j=1}^{m}k(y_i,y_j). \tag{7}$$

Here, $k$ is the Gaussian kernel function, that is, $k(x, y) = \exp(-\|x - y\|^2/(2\sigma^2))$. The distance between two distributions can be calculated using the inner product. For ease of computation on a computer, this can be simplified to Eq. (10).

$$MMD_k(X,Y) = tr\left(\begin{bmatrix} K_{X,X} & K_{X,Y} \\ K_{Y,X} & K_{Y,Y} \end{bmatrix} M\right), \tag{8}$$

where $M$ is

$$M_{ij} = \begin{cases} \dfrac{1}{n^2}, & x_i, x_j \in X \\ \dfrac{1}{m^2}, & y_i, y_j \in Y \\ -\dfrac{1}{nm}, & \text{otherwise} \end{cases}. \tag{9}$$

The final goal of the improved sparse denoising self-encoder is defined as

$$J_{ISDAE}(W,b) = \frac{1}{2m}\sum_{i=1}^{m}(\| h_{W,b}(\tilde{x})^{(i)} - y^{(i)} \|^2) + \beta\sum_{j=1}^{s_1} KL(\rho \| \hat{\rho}_j) + MMD_k(X,Y). \tag{10}$$

Overall, the raw data is denoised using a denoising AE, which effectively removes noise. Add a sparsity penalty term in the AE to ensure sparse activation in the hidden layer. Incorporate an MMD penalty term in the loss function to enhance distribution alignment across different sensor data. Train the AE model using the improved loss function, optimizing model parameters through backpropagation. Extract key features from the preprocessed data for further fault diagnosis and identification.

### 2.2 Self-attention mechanism

The attention mechanism enables models to focus on specific parts of the input data while disregarding less relevant parts. This is achieved by calculating dynamic weights based on the information in the sequence. Consequently, each model incrementally learns which parts of the sequence are crucial for understanding as it processes the sequence.

In the research advancements of attention mechanisms, spatial attention and channel attention have garnered significant attention. In this section, we describe the use of a hybrid attention module based on an attention mechanism, as illustrated in Fig. 6. The module is based on the convolutional block attention module (CBAM) proposed by Woo *et al.*,[14] which integrates spatial attention and channel attention. However, the weights for spatial attention and channel attention should not be identical owing to the complexity and redundant computations in the process, which is disadvantageous for real-time bearing fault diagnosis under variable operating conditions. Consequently, a more flexible approach is proposed to fine-tune the feature mappings extracted by the attention mechanism. The two branches of the attention module have been redesigned for enhanced adaptability.

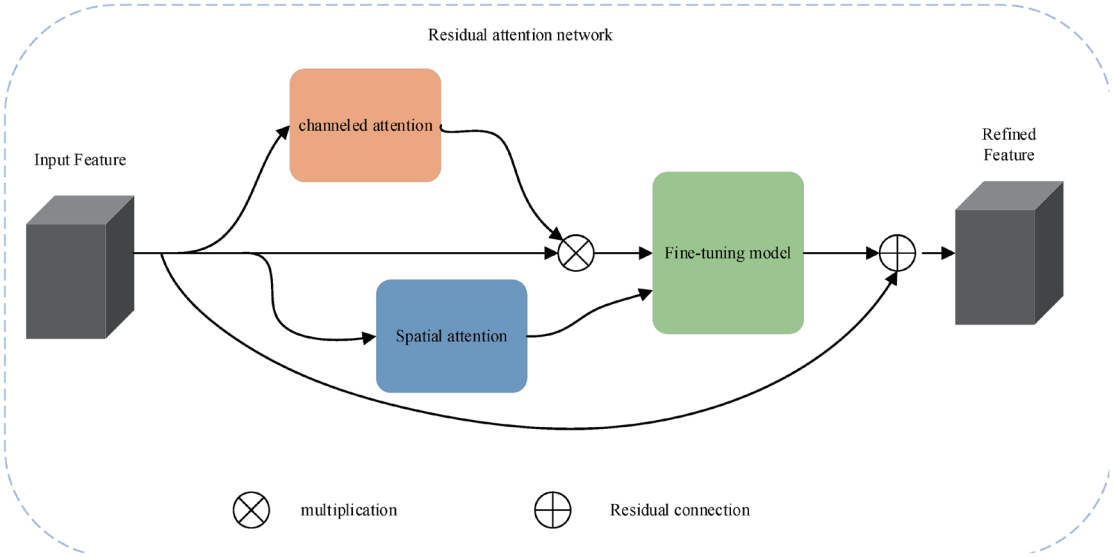


Fig. 6. (Color online) Hybrid attention module.

For a single attention module, the mechanism operates via Eq. (10). A parallel structure is used where $F_{input}$ is the input feature mapping; $F_{input} \in R^{c \times w \times h}$. The attention module generalizes the 1D channel attention map $F_c \in R^{c \times 1 \times 1}$ and the 2D spatial attention feature map $F_s \in R^{l \times w \times h}$. For the channel attention branch, the tensor is shown in Eq. (13).

$$F_{output} = (F_c + F_s) \otimes F_{input} \tag{11}$$

In Eq. (11), the operation denoted by ⊗ refers to elementwise multiplication, indicating that the adjustments depend on iterative variations. During this computational process, spatial attention and channel attention are concurrently calculated and integrated through a concatenation operation, thereby enhancing the diversity of feature mappings. This approach facilitates adequate information extraction even from a limited dataset. Furthermore, to accommodate the diversity of target objectives, a more flexible spatial attention branch structure has been conceptualized, as shown in Fig. 7. The spatial attention module is described by Eq. (12), where $x$ represents the input feature map, $S_{max}(x)$ the feature map following maximum pooling, and $S_{avg}(x)$ the result of average pooling. A regulator, as demonstrated in the figure, is defined by Eqs. (13) and (14), incorporating the nonlinear functions $S_1(T)$ and $S_2(T)$. The parameter $T$, which is dependent on iteration changes, is designed to modulate the feature extractor. This parameter $T$ signifies the adjustments reliant on iterative variations.

$$F_s = \frac{S_{max}(x) + S_{avg}(x)}{2} + S_1(T) * S_{max}(x) + S_2(T) * S_{avg}(x) \tag{12}$$

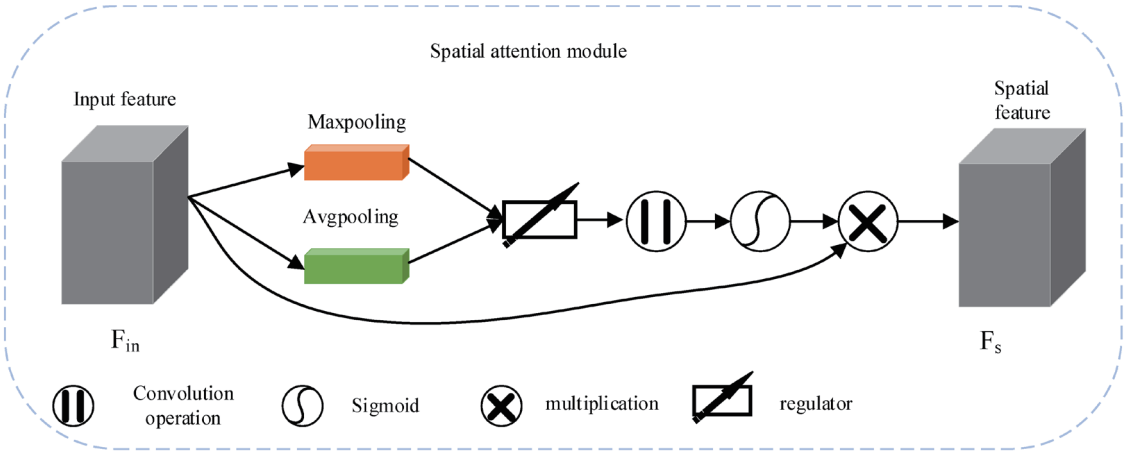


Fig. 7. (Color online) Spatial attention module.

$$S_1(T) = \begin{cases} -0.5, & epoch < T \\ 0.5, & epoch \geq T \end{cases} \tag{13}$$

$$S_2(T) = \begin{cases} 0.5, & epoch < T \\ -0.5, & epoch \geq T \end{cases} \tag{14}$$

The spatial attention mechanism in this study focuses on key pixel regions in images crucial for classifiers, enhancing the neural network's ability to perceive important areas in images and thereby improving the accuracy of image classification. We have optimized the architecture of the squeeze-and-excitation (SE) network in this research. As demonstrated in Fig. 8, additional global max pooling operations were implemented to effectively extract more channel information from individual layers. Furthermore, to enhance feature extraction, we innovatively integrated two branches of channel attention modules. These attention modules were effectively embedded into the foundational backbone network. The network constructed in this study includes three convolutional layers in residual blocks and four enhanced residual attention blocks, forming a 12-layer deep residual attention network.

## 2.3 Multisensor fusion technology

Multisensor fusion, also known as multisensor information fusion, was first proposed in 1973 in the sonar signal processing system developed by the U.S. Department of Defense. It processes and synthesizes the information from the perspective of multiple information, and obtains the intrinsic connection and law of various types of information, so as to eliminate useless and erroneous information, retain the correct and useful components, and ultimately realize the optimization of the information.

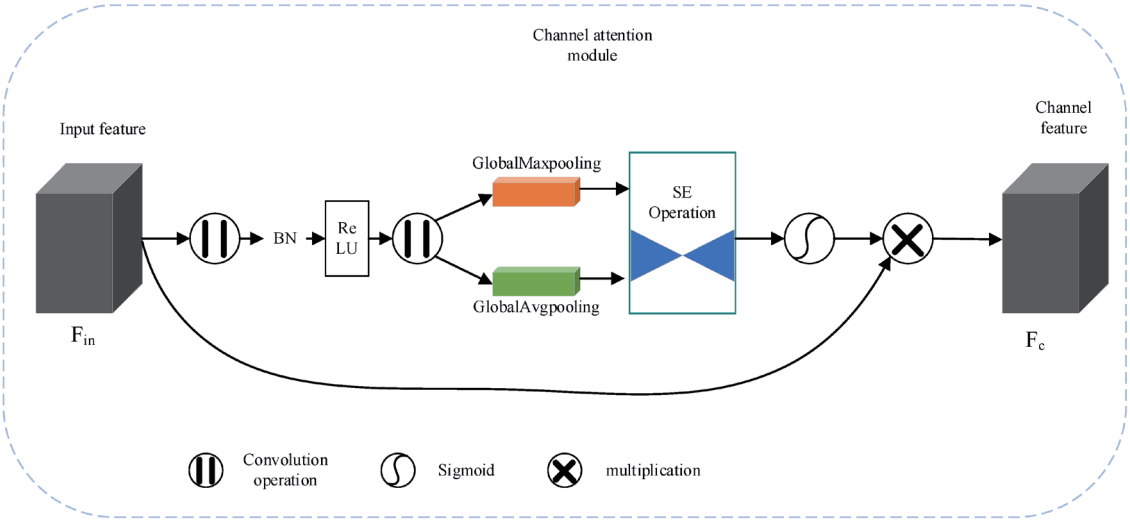


Fig. 8. (Color online) Channel attention module.

Multisensor fusion is structurally divided into three main layers according to its abstraction layer of information processing in the fusion system: data layer fusion, feature layer fusion, and decision layer fusion.

(1) Data layer fusion: Also known as pixel-layer fusion, it first fuses the observed data from the sensors, then extracts the feature vectors from the fused data and performs judgmental recognition. Data layer fusion requires that the sensors be homogeneous (the sensors observe the same physical phenomenon). If multiple sensors are heterogeneous (the observation is not the same physical quantity), then the data can only be fused in the feature or decision layer. The data layer fusion does not have the problem of data loss and the results obtained are accurate, but it is computationally intensive and requires a high communication bandwidth for the system.

(2) Feature layer fusion: Feature layer fusion belongs to the intermediate layer, where representative features are first extracted from the observation data provided by each sensor, and these features are fused into a single feature vector, which is then processed using pattern recognition methods. The computation and the requirement of communication bandwidth are lower in this method, but the accuracy is reduced by the abandonment of part of the data.

(3) Decision layer fusion: Decision layer fusion is a high-layer fusion that produces relatively inaccurate results because of the condensation of the sensor data.

## 3. Bearing Fault Diagnosis Method Based on DR-MLDSO

### 3.1 DR-MLDSO bearing diagnostics methodology framework

The DR-MLDSO-based bearing fault diagnosis method preprocesses and reconstructs data using an improved encoder. It employs an enhanced ResNet18 network combined with a hybrid dual-channel attention mechanism for deep feature extraction. The method uses MMD to align the distribution of data from different sensors to optimize the feature space, and finally classifies faults through a fully connected layer. This approach incorporates an improved SDAE to reconstruct vibration signal data, thereby reducing noise impact. The meta-learning model extracts key features and patterns from data through convolution and normalization, and optimizes the discriminative space to reduce intraclass distance and increase interclass distance, enhancing classification accuracy. The introduction of a self-attention mechanism allows DR-MLDSO to adaptively focus on more relevant parts, further improving diagnostic accuracy. This model boasts strong noise handling capability, excellent feature extraction, outstanding data fusion ability, and superior classification performance. It performs exceptionally well with small sample sizes and under variable working conditions, demonstrating high adaptability and robustness. The structure of DR-MLDSO is shown in Fig 9.

### 3.2 DR-MLDSO bearing fault parameter diagnosis

In meta-learning-based bearing fault diagnosis, the feature extraction component is crucial. The variable condition bearing fault diagnosis method based on DR MLDSO selects ResNet as the primary feature extraction network with its structure depicted in Fig. 10. The feature

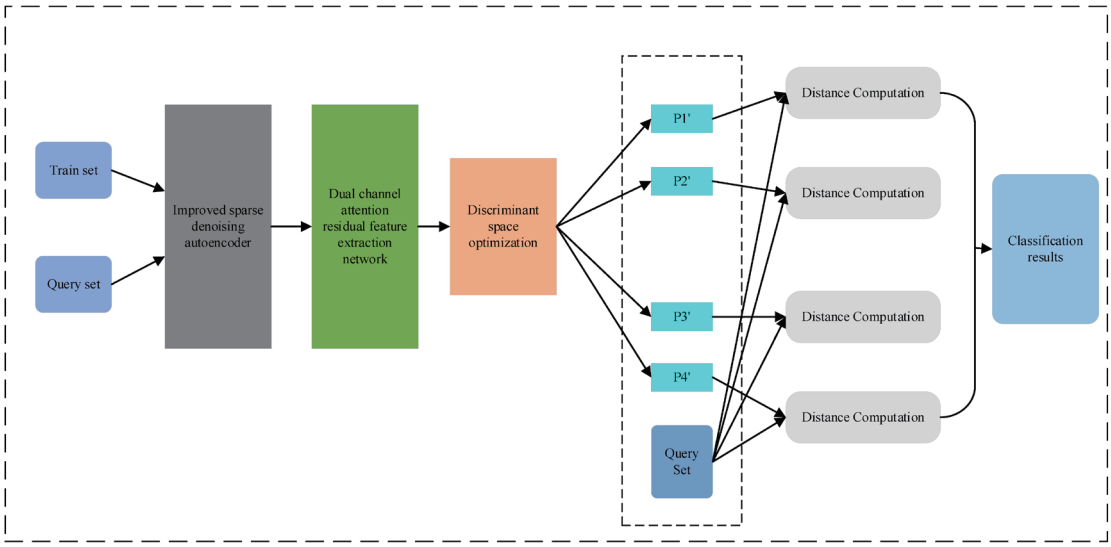


Fig. 9. (Color online) Structure of DR-MLDSO.

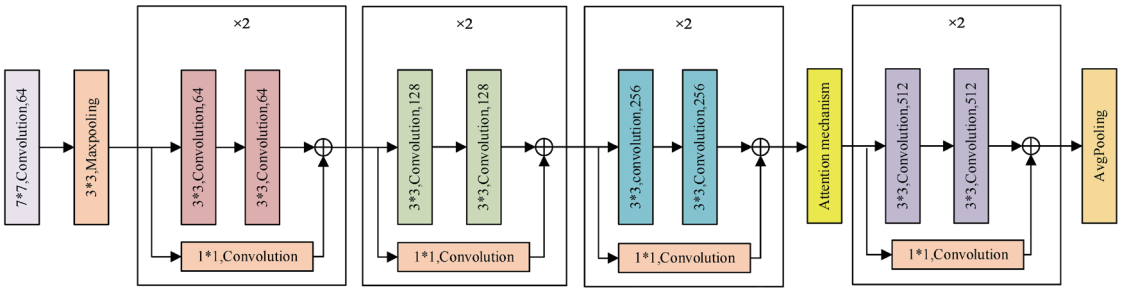


Fig. 10. (Color online) Structure diagram of feature extraction module.

extraction network is divided into four modules; specifically, modules 1 to 4 are each composed of two residual blocks connected in series. Additionally, a hybrid attention module is introduced between modules 3 and 4. During the model training phase, source and target domain data are processed through 7 × 7 convolution and 3 × 3 max pooling, and subsequently inputted into these four modules for feature extraction. Finally, the extracted features undergo average pooling to reduce the number of parameters, and then they are transformed into 1D vectors through a fully connected (FC) layer to facilitate subsequent discriminative space optimization.

In the variable-condition bearing fault diagnosis method based on DR-MLDSO, 1D vibration signals are initially transformed into 2D grayscale images. These images then undergo data reconstruction to mitigate the impact of noise on diagnostic accuracy. ResNet18 is selected as the feature extraction network, effectively extracting relevant features. Subsequently, the extracted features are subjected to discriminative space optimization, enhancing the network's nonlinear fitting capability for fault diagnosis in small sample situations. The proposed process for variable-condition bearing fault diagnosis based on small-sample meta-learning is depicted in Fig. 11, where FC denotes a fully connected layer. The entire fault diagnosis process is divided into three stages: data preprocessing, offline modeling, and online diagnosis.

## 4. Experimental Results

### 4.1 Experimental preparation and dataset introduction

In this experiment, we utilized two datasets from Case Western Reserve University (CWRU)[15] and Southeastern University (SEU).[16] The CWRU dataset includes 10 sets of data, with healthy data collected at 48 kHz, 1772 rpm, and a load of 1. The fault data are categorized on the basis of fault diameters of 0.007, 0.014, and 0.021 inches. The SEU dataset consists of motor bearing data, with a speed of 20 Hz, with a load configuration of 2, and fault categories including rolling element cracks, inner ring cracks, inner and outer ring cracks, and healthy data.

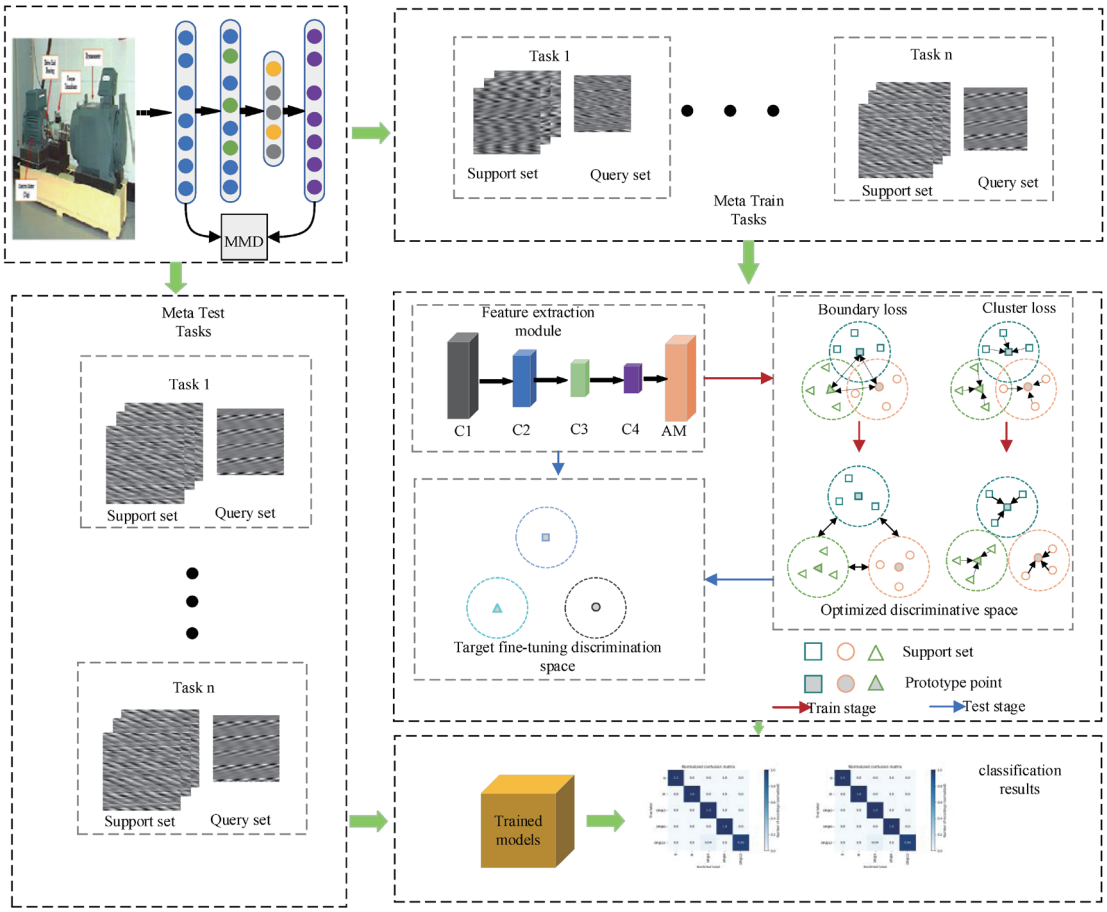


Fig. 11. (Color online) Rolling bearing fault diagnosis flow chart based on DR-MLDSO.

## 4.2 Experimental method

This section is focused on bearing fault diagnosis under variable working conditions using the DR-MLDSO method, with experiments conducted using the CWRU and SEU datasets. In these experiments, the loss parameter $\beta$ of the DR-MLDSO method was set to 0.00005. Additionally, the learning rate was fixed at 0.001, and the Adam optimizer was selected for all methods to optimize performance. To reduce experimental error, each experiment was repeated 10 times, with the minimum and maximum values discarded. The average of the remaining eight trials was used as the final evaluation result.

The software used for data processing in the model was Matlab2018b. The computer configuration for testing the model included the following: CPU: Intel i7-8700, 3.2 GHz, 6 cores, 12 threads; GPU: NVIDIA GeForce GTX 1080Ti. The software frameworks used were Python 3.6.6 and Python 1.2.0.

### 4.3 Experimental data validation

To validate the model's performance in real industrial environments, noise processing was conducted to simulate noise interference. Twelve operational condition transfer tasks were designed to test the model's generalization ability, and the training and testing times of the model were evaluated to verify its real-time performance and feasibility in industrial applications. The design of task transfer and small sample size learning validated the model's rapid adaptability and efficient diagnostic capability under different conditions. In these designations, for example, A-B indicates that data from condition A serves as the source domain, while data from condition B is treated as the target domain. The specific settings for these variable-condition samples are detailed in Table 1.

#### 4.3.1 CWRU fault diagnosis study on bearing dataset under variable operating conditions

To simulate real-world conditions more accurately, the CWRU dataset was subjected to noise processing, including −13 dB salt and pepper noise and −2 dB Gaussian white noise. We designated the original denoised CWRU dataset as M0, the CWRU dataset with −13 dB salt and pepper noise as M1, and the CWRU dataset with -13 dB salt and pepper noise and −2 dB Gaussian white noise as M2. From M0, M1, and M2, we selected 80% of the 2D grayscale images to create n-way k-shot tasks for training and reserved 20% of the grayscale images for testing.

Experiment 1: To demonstrate the effectiveness of the DR-MLDSO method in bearing fault diagnosis under variable operating conditions, we compared it with DAN, DANN, PrototypeNet, RelationNet, MAML, MTL, MLDSO, and DR-MLDSO models. We randomly selected five categories from each subset and chose five samples from each category for training the 5way-5shot model. One sample per category was selected randomly for training Model 5way-1shot.The experimental outcomes are presented in Tables 2 and 3, which conform to the same parameter settings as in the DR-MLDSO model.

From Table 2 and Fig. 12, it is evident that the DR-MLDSO model has the highest average accuracy under 5way-5shot, surpassing the second-highest accuracy of the MLDSO model by 2.94% and the lowest one of the DAN model by 13.12%. This indicates that the DR-MLDSO model can be used for the diagnosis of bearing faults under variable operating conditions with high accuracy. Moreover, the mean accuracy of fault diagnosis achieved by the MLDSO model significantly exceeds those of the DAN, DANN, Prototype Net, Relation Net, MAML, and MTL models. DR-MLDSO demonstrates that ISDAE's denoising, sparse representation, and

Table 1
CWRU sample settings for variable conditions.

| | Task | | | | | | | | | | | |
|---|---|---|---|---|---|---|---|---|---|---|---|---|
| | 1 | 2 | 3 | 4 | 5 | 6 | 7 | 8 | 9 | 10 | 11 | 12 |
| Migration Task | A-B | A-C | A-D | B-A | B-C | B-D | C-A | C-B | C-D | D-A | D-B | D-C |
| Source Domain | A | A | A | B | B | B | C | C | C | D | D | D |
| Target Domain | B | C | D | A | C | D | A | B | D | A | B | C |

Table 2
CWRU (5way-5shot) experimental results under variable working conditions (%).

| | DAN | DANN | MAML | Relation Net | Prototype Net | MTL | MLDSO | DR-MLDSO |
|---|---|---|---|---|---|---|---|---|
| A-B | 88.25 | 90.96 | 86.66 | 92.03 | 91.29 | 93.85 | 94.14 | 95.92 |
| A-C | 88.79 | 82.79 | 90.93 | 91.25 | 89.35 | 91.26 | 95.23 | 98.14 |
| A-D | 84.25 | 78.57 | 86.66 | 88.69 | 90.64 | 87.71 | 94.88 | 98.71 |
| B-A | 90.32 | 87.16 | 89.06 | 90.46 | 92.57 | 93.12 | 92.51 | 97.61 |
| B-C | 93.76 | 90.85 | 86.93 | 91.77 | 90.62 | 97.64 | 96.89 | 99.64 |
| B-D | 88.34 | 91.22 | 76.00 | 85.19 | 92.36 | 93.86 | 97.24 | 97.86 |
| C-A | 77.56 | 86.34 | 73.61 | 83.25 | 89.61 | 92.45 | 94.53 | 97.45 |
| C-B | 80.26 | 92.44 | 88.38 | 90.46 | 94.24 | 95.79 | 97.12 | 99.79 |
| C-D | 85.36 | 93.42 | 95.20 | 89.75 | 95.16 | 96.74 | 94.58 | 98.74 |
| D-A | 81.72 | 73.22 | 76.10 | 85.49 | 89.98 | 90.67 | 96.33 | 97.13 |
| D-B | 77.54 | 82.07 | 89.66 | 91.46 | 96.26 | 93.54 | 94.74 | 98.54 |
| D-C | 84.15 | 85.65 | 89.86 | 92.67 | 97.29 | 92.21 | 94.29 | 98.28 |
| Average | 85.03 | 86.22 | 85.75 | 89.37 | 92.45 | 93.24 | 95.21 | 98.15 |

Table 3
CWRU (5way-1shot) experimental results under variable working conditions (%).

| | DAN | DANN | MAML | Relation Net | Prototype Net | MTL | MLDSO | DR-MLDSO |
|---|---|---|---|---|---|---|---|---|
| A-B | 78.83 | 75.37 | 79.54 | 76.94 | 87.05 | 87.73 | 88.41 | 89.62 |
| A-C | 72.45 | 76.28 | 89.60 | 88.05 | 87.52 | 85.60 | 91.30 | 92.61 |
| A-D | 69.54 | 75.25 | 79.46 | 82.71 | 84.01 | 86.77 | 92.48 | 95.32 |
| B-A | 74.94 | 72.15 | 82.53 | 89.64 | 90.11 | 75.34 | 91.58 | 94.43 |
| B-C | 79.48 | 87.99 | 86.64 | 82.98 | 87.61 | 93.32 | 90.85 | 92.23 |
| B-D | 67.40 | 76.59 | 82.14 | 85.39 | 85.45 | 87.75 | 95.24 | 97.55 |
| C-A | 65.56 | 72.85 | 70.26 | 72.63 | 83.05 | 80.37 | 92.63 | 94.45 |
| C-B | 80.84 | 74.19 | 87.48 | 88.56 | 87.74 | 92.50 | 95.12 | 95.33 |
| C-D | 72.56 | 87.54 | 73.01 | 75.25 | 83.76 | 91.18 | 95.46 | 96.18 |
| D-A | 64.35 | 77.63 | 83.73 | 81.21 | 85.66 | 76.30 | 95.33 | 97.03 |
| D-B | 74.46 | 75.30 | 90.66 | 88.64 | 89.26 | 85.45 | 94.24 | 96.35 |
| D-C | 82.27 | 86.77 | 82.59 | 85.76 | 88.65 | 88.46 | 95.25 | 97.28 |
| Average | 73.56 | 78.16 | 82.30 | 83.15 | 86.66 | 85.90 | 93.16 | 94.87 |

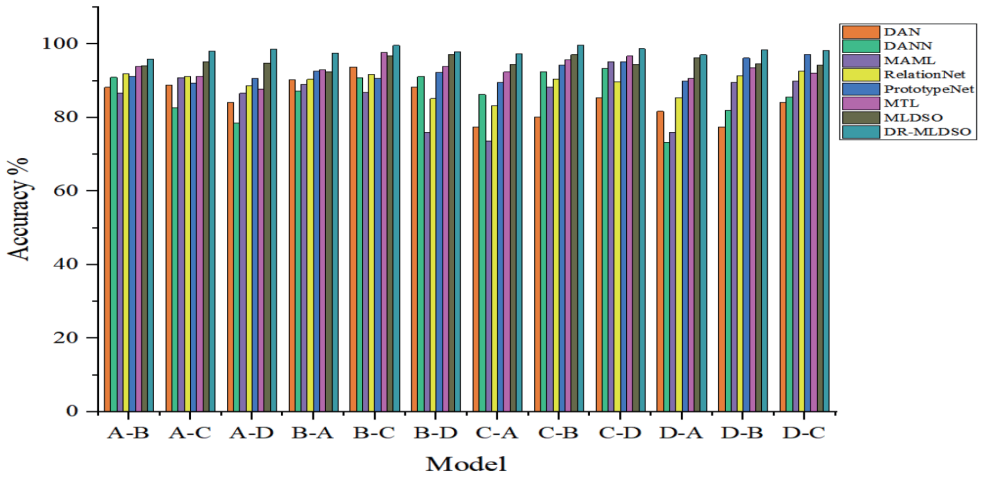


Fig. 12. (Color online) CWRU variable-condition contrast experiment results.

cooperative distribution abilities generate valuable information in the reconstructed data. In addition, the self-attention mechanism enhances the model's focus on useful information, enabling similar fault features to be clustered and different categories of fault features to be separated, thereby improving the fault diagnosis of bearings under variable operating conditions and enhancing its accuracy.

From Table 3, it is evident that the DR-MLDSO model has the highest average accuracy under 5way-1shot, surpassing the second-highest average accuracy of the MLDSO model by 1.68% and the lowest one of the DAN model by 98.15%. This indicates that the DR-MLDSO model can be used for the diagnosis of bearing faults under variable operating conditions with high accuracy. The average accuracies stand at 94.87% for 5way-1shot and 98.15% for 5way-5shot, which surpasses the performance of the remaining four models.

In twelve different operating condition transfer tasks, the DR-MLDSO model generally performs excellently. For instance, in tasks A-B and D-C, the diagnostic accuracies of the DR-MLDSO model are 95.92 and 98.28%, respectively, demonstrating a stronger diagnostic capability. The DR-MLDSO model was compared with various existing methods, including DAN, DANN, MAML, RelationNet, PrototypeNet, and MLDSO. The results show that DR-MLDSO achieves a higher diagnostic accuracy under most operating conditions than other methods. This indicates that although these other methods have advantages in handling small sample data, they are less effective than DR-MLDSO in dealing with complex conditions and noise interference.

Additionally, the accuracy of the 5shot model is superior to that of the 1shot model. This result can be attributed to the increased comprehensive fault information and features present in the 5-shot model, which enhances its generalization ability. Moreover, the model proposed in this paper extracts more and better features for diagnosis, thereby reducing overfitting.

Experiment 2: To further validate the effectiveness of the proposed method in fault misclassification, confusion matrix experiments were conducted on the DRMLDSO and MLDSO models using the M1 dataset, where the a-axis is the predicted value and the b-axis is the true value. Four working conditions, A-B, A-C, A-D, and D-C of DR-MLDSO and A-D and D-C of MLDSO, were selected to apply the confusion matrix and feature embedding space of different meta-learning methods visualized with t-SNE to check the reliability of the results. The results are shown in Fig. 13.

From Fig. 13, it is evident that the DR-MLDSO model can effectively discriminate the faults of each category for the three variable conditions A-B, A-C, and A-D, which indicates that the DR-MLDSO model can discriminate well the confusion between the faults. As shown in Fig. 13(d), MLDSO misclassified 0.007OR and 0.021IR during A-D state migration. From the embedded feature space, it can be seen that these two defect features overlap with other feature categories, resulting in their classification in a variable-condition noise environment. The DR-MLDSO in Fig. 13(c) has a fault identification rate of 100% for A-D migration. In Fig. 13(e), 3% of 0.014IR is identified as 0.021IR, and the remaining faults are identified with 100%, whereas in Fig. 13(f), only four types of fault are identified with 100%, and the remaining faults are identified with 100%. This indicates that adding data reconstruction and hybrid dual-channel attention to MLDSO can improve the effectiveness of the model in fault detection.

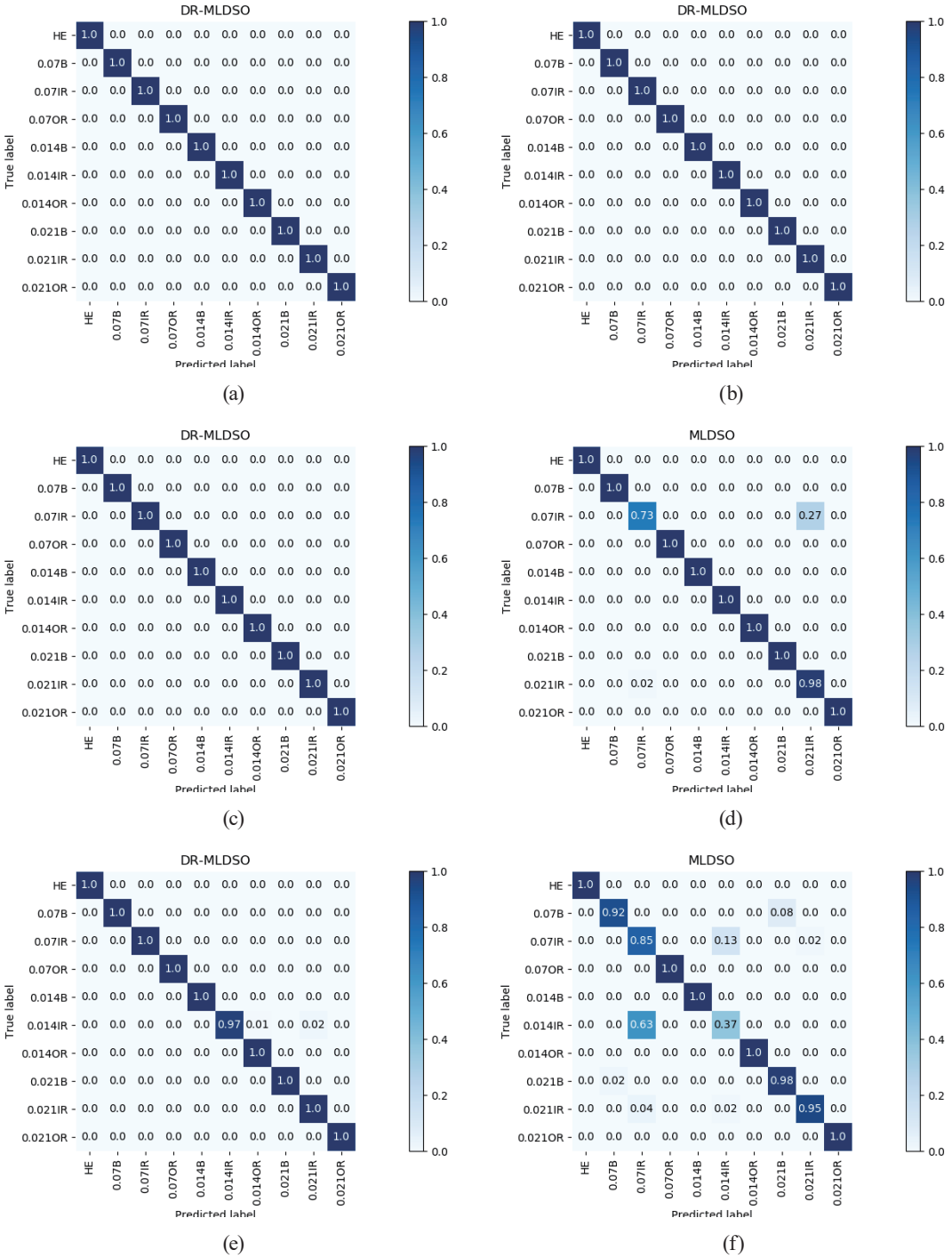


Fig. 13. (Color online) Confusion matrices. Working conditions of (a) DR-MLDSO A-B, (b) DR-MLDSO A-C, (c) DR-MLDSO A-D, (d) MLDSO A-D, (e) DR-MLDSO D-C, and (f) MLDSO D-C.

Experiment 3: Bearing failures can occur instantaneously in real industrial applications, demanding a high layer of real-time performance of fault diagnosis methods. Hence, assessing the feasibility of the proposed DR-MLDSO technique for industrial applications is crucial. In this section, we examine the training time and testing time of the DR-MLDSO model to confirm

its practicality when the training set size is fixed at 20 samples per class and 5way-5shot tasks are used. The analysis aims to validate the feasibility of the model's application. To ensure that the experiment is reliable, the model is trained from the initial epoch until fitting completion and tested using input data samples until prediction result generation. WDCNN, RelationNet, PrototypeNet, MAML, MLDSO, and DR-MLDSO are utilized, and the experimental outcomes are presented in Table 4, Fig. 14, and Fig. 15.

Specifically, WDCNN, PrototypeNet, RelationNet, MLDSO, and DR-MLDSO exhibit swift training times owing to the small training set size and ease of model fitting. On the other hand, MAML takes more time owing to the larger training shipment. PrototypeNet shows the shortest training period because it is simple and efficient, and can easily be optimized in terms of its design. Because of the design of the loss function and self-attention mechanism in the proposed DR-MLDSO method, the training time is slightly longer than that of PrototypeNet. Nevertheless, the increase in training period is tolerable in light of the enhanced accuracy achieved. Furthermore, the DR-MLDSO method's test time is found to be within 1 ms, on par with those of the DAN, DANN, PrototypeNet, and MAML models. Conversely, both RelationNet and WDCNN exhibit test times exceeding 1 ms. Despite a small reduction in training time, the fault diagnosis accuracy is significantly enhanced, with each sample test time falling below 1ms. The system's real-time performance is commendable, and the findings demonstrate that the technique can accomplish the instantaneous diagnosis of bearing malfunctions.

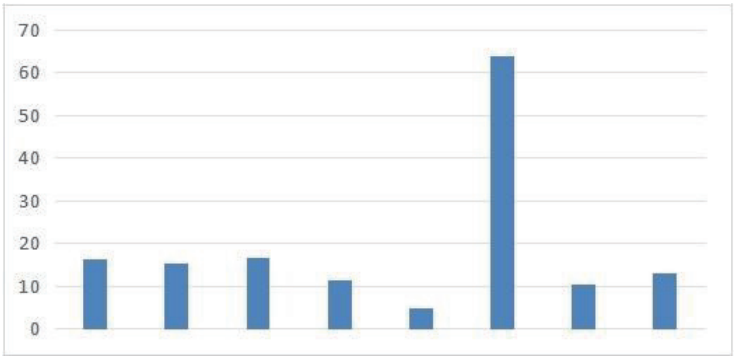


Fig. 14. (Color online) Training time of each model.

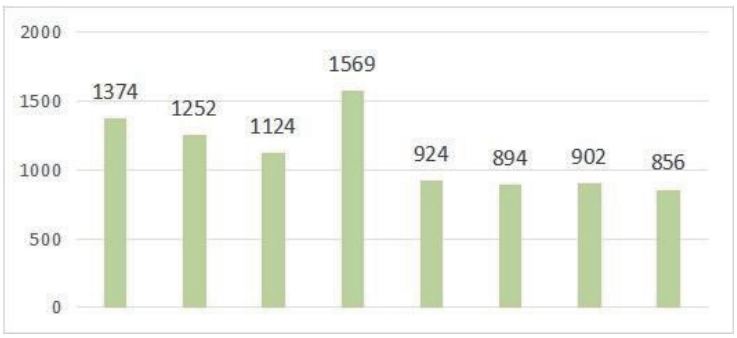


Fig. 15. (Color online) Test time of each model.

Table 4
Training time and test times (%).

| | DAN | DANN | WDCNN | Relation Net | Prototype Net | MAML | MLDSO | DR-MLDSO |
|---|---|---|---|---|---|---|---|---|
| Train/s | 16.21 | 15.22 | 16.85 | 11.54 | 4.94 | 64.05 | 10.41 | 13.24 |
| Test/us | 1374 | 1252 | 1124 | 1569 | 924 | 894 | 902 | 856 |

Table 5
SEU variable-condition sample settings.

| | Migration Task | Source Domain | Target Domain | Source Domain samples/per | Target Domain samples/per |
|---|---|---|---|---|---|
| Task 13 | E-F | E | F | 400 | 400 |
| Task 14 | F-E | F | E | 400 | 400 |

Table 6
SEU L0 experiment results under variable working conditions.

| | DAN | DANN | RelationNet | MAML | MLDSO | DR-MLDSO |
|---|---|---|---|---|---|---|
| E-F | 87.00 | 86.34 | 94.17 | 95.50 | 98.76 | 99.38 |
| F-E | 85.21 | 89.75 | 93.59 | 91.00 | 97.62 | 99.79 |
| Average | 86.11 | 88.05 | 93.88 | 93.25 | 98.19 | 99.59 |

### 4.3.2 SEU experiment on fault diagnosis of motor bearing dataset under variable operating conditions

To assess the generalizability of the proposed bearing fault diagnosis method under variable working conditions based on DR-MLDSO, experiments were conducted using the ML electric motor bearing fault dataset. We set the original noise-free dataset of ML motor bearings as L0, the bearing dataset with -13 dB salt and pepper noise as L1, and the bearing dataset with -13 dB salt and pepper noise plus -2 dB Gaussian white noise as L2. The detailed configurations of the variable operating conditions in the ML dataset are shown in Table 5.

Experiment 4: To corroborate the efficacy of the proposed DR-MLDSO method, we implemented the DAN, DANN, RelationNet, MAML, MLDSO, and DR-MLDSO models for bearing fault diagnosis under variable operating conditions, specifically in the L0 scenario utilizing a 5way-5shot approach. The results of this experiment are comprehensively documented in Table 6.

According to Table 6, the average fault diagnosis accuracies for the DAN, DANN, RelationNet, MAML, MLDSO, and DR-MLDSO models are 86.11, 88.05, 93.88, 93.25, 98.19, and 99.59%, respectively. Notably, the DR-MLDSO model achieved the highest average fault diagnosis accuracy, surpassing the second-highest value of the MLDSO model by 1.40% and outperforming the lowest-ranked MAML model by 6.34%. This indicates that the DR-MLDSO model significantly enhances the accuracy of bearing fault diagnosis under variable working conditions.

Experiment 5: To verify the superiority of the DR-MLDSO method in bearing fault diagnosis under noisy conditions, we conducted bearing fault diagnosis under variable operating conditions

Table 7
SEU L1 experimental results under variable working conditions (%).

| | DAN | DANN | RelationNet | MAML | MLDSO | DR-MlLDSO |
|---|---|---|---|---|---|---|
| E-F | 81.04 | 80.37 | 81.71 | 83.54 | 94.73 | 98.34 |
| F-E | 77.29 | 82.45 | 79.25 | 84.00 | 95.62 | 98.75 |
| Average | 79.17 | 81.41 | 80.48 | 83.77 | 95.18 | 98.55 |

Table 8
SEU L2 experimental results under variable working conditions (%).

| | DAN | DANN | RelationNet | MAML | MLDSO | DR-MLDSO |
|---|---|---|---|---|---|---|
| E-F | 74.87 | 77.ZJ | 76.21 | 79.50 | 93.45 | 96.37 |
| F-E | 73.15 | 74.25 | 77.63 | 78.00 | 92.27 | 94.25 |
| Average | 74.01 | 75.74 | 76.92 | 78.75 | 92.86 | 95.31 |

for the 5way-5shot task in the L1 and L2 datasets using the DAN, DANN, RelationNet, MAML, MLDSO, and DR-MLDSO models. The other model parameter settings are the same as those for DR-MLDSO. The experimental results shown in Tables 7 and 8 reveal that the DR-MLDSO model has the highest average accuracy in both the L1 and L2 datasets. The decrease in accuracy is small under both L1 and L2 conditions, which indicates that the DR-MLDSO model possesses superior noise resistance capabilities.

## 5. Conclusions

In this paper, we introduced a novel bearing fault diagnosis method under variable working conditions, based on DR-MLDSOD, to address the challenge of low accuracy in bearing fault diagnosis under such conditions. An improved SDAE was developed to reconstruct the acquired data. The method involves adjusting the distribution of subdomains related to domain-specific layer activations across different domains. It employs a method based on MMD to enhance the feature representation ability of the meta-learning network and align it with the relevant subdomain distributions. Finally, a hybrid dual-channel attention mechanism is integrated into the improved residual network to increase the focus on local features. The method was tested for variable-condition bearing fault diagnosis on the CWRU and SEU datasets.

The experimental results illustrate that the DR-MLDSO model achieves a higher accuracy in fault diagnosis than do other models under variable operating conditions and noisy environments. This method considerably alleviates the impact of variable operating conditions and noise interference on diagnostic accuracy in small sample situations and improves diagnostic accuracy in such environments.

The DR-MLDSO model exhibits excellent performance in bearing fault diagnosis. However, practical applications should consider limitations such as computational resource requirements, training time, data quality dependency, adaptability, hyperparameter tuning, and data fusion. These factors can complicate the application and deployment of the model. Additionally, the effectiveness and feasibility of the model in real industrial environments should be tested.

## Acknowledgments

This work is supported by the Science and Technology Foundation of Liaoning Province Education Department of China under Grant JYTZD2023006. This research project is Liaoning Provincial Department of Education Scientific Research Project Plan "Research on Complex Process Set Fault Diagnosis Method Based on Meta Learning Network".

## References

1 Q. Q. Chen, S. W. Dai, and H. D. Dai: Instrum. Technol. **9** (2019) 1. https://doi.org/10.19432/j.cnki.issn1006-2394.2019.09.001
2 Q. Yang, J. Y. Zhang, and D. S. Wu: Bearing **8** (2021) 39. https://doi.org/10.19533/j.issn1000-3762.2021.08.008
3 Q. Yang, J. G. Lu, and X. H. Tang: J. Ordnance Equip. Eng. **42** (2021) 235.
4 W. Li, Z. Shang, M. Gao, S. Qian, B. Zhang, and J. Zhang: Eng. Appl. Artif. Intell. **102** (2021) 104279.
5 R. M. Hasani, G. Wang, and R. Grosu: arXiv **1703** (2017) 06272. https://doi.org/10.48550/arXiv.1703.06272
6 W. Zhang, C. H. Li, G. L. Peng, Y. H. Chen, and Z. J. Zhang: Mech. Syst. Signal Process. **100** (2018) 439.
7 D. Hoang, and H. Kang: Cognit. Syst. Res. **53** (2019) 42.
8 C. Finn, P. Abbeel, and S. Levine: 34th Int. Conf. Mach. Learn. (International Machine Learning Society, IMLS) **70** (2017) 1126–1135.
9 A. Zhang, S. Li, Y. Cui, W. Yang, R. Dong, and J. Hu: IEEE Access (2019) 110895. https://doi.org/10.1109/ACCESS.2019.2934233
10 J. Snell, K. Swersky, and R. Zemel: Adv. Neural Inf. Process Syst. **30** (2017) 4078.
11 D. Wang, M. Zhang, Y. Xu, W. Lu, J. Yang, and T. Zhang: Signal Process **155** (2021) 107510.
12 P. Shi, X. Guo, D. Han, and R. Fu: Mech. Sci. Technol. **34** (2020) 1445. https://doi.org/10.1007/s12206-020-0306-1
13 Z. Meng, X. Zhan, J. Li, and Z. Pan: Measurement **130** (2018) 448.
14 S. Woo, J. Park, J. Y Lee: Proc. European Conf. Computer Vision (ECCV, 2018) 3–19. https://doi.org/10.1007/978-3-030-01234-2_1
15 Case Western Reserve University. Bearing Data Center [DB/OL] https://csegroups.case.edu/bearingdatacenter/home (Accessed September 2020).
16 Southeast University. ML Mechanics Portal: Mechanical Dataset [DB/OL] https://mlmechanics.ics.uci.edu. (Accessed December 2019).

## About the Authors

**Dongsheng Wu** received his B.S. and M.S. degrees from Shenyang Institute of Technology, China, in 1997 and 2005, respectively, and his Ph.D. degree from Changchun University of Science and Technology, China, in 2013. From 2013 to 2019, he was an assistant professor, and since 2020, he has been a professor at Shenyang Ligong University. His research interests are in intelligent control, fault diagnosis, and sensors. (wuds@sylu.edu.cn)

**Yihao Chen** received his B.S. degree from Shenyang Institute of Urban Construction, China, in 2022, and in the same year, he started studying for a master's degree in Shenyang Polytechnic University. His research interests are in deep learning, fault diagnosis, and sensors. (cyh541877@163.com)

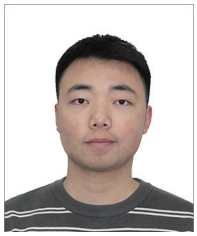

**Yifan Chen** received his B.S. degree in automation from Beijing Jiaotong University, Haibin College, China, in 2020 and his M.S. degree in intelligent systems from Shenyang Ligong University, China, in 2023. He is currently working on his Ph.D. degree in intelligent robotics at the University of Portsmouth, U.K. His research interests include facial recognition, human motion analysis, and human–robot collaboration. (yifan.chen@port.ac.uk)